Wheel-INS: A Wheel-mounted MEMS IMU-based Dead Reckoning System

Xiaoji Niu, Yibin Wu and Jian Kuang

***Abstract*—To improve the accuracy and robustness of microelectromechanical system (MEMS) inertial measurement units (IMU)-based inertial navigation systems (INSs) for wheeled robot localization without adding cost, a complete wheel-mounted MEMS IMU (Wheel-IMU) based dead reckoning system (Wheel-INS) is proposed in this study. The installation scheme of the Wheel-IMU, algorithm structure, and error analysis are explained. In Wheel-INS, a MEMS-IMU is placed at the center of a non-steering wheel of the wheeled robot to take advantages of rotation modulation; gyroscope measurements are then used to calculate the wheel velocity to mitigate the error drift of INS along with the vehicle motion constraints through an extended Kalman filter. Experimental results show that Wheel-INS is insensitive to gyroscope bias error. The maximum position drift in the horizontal plane of the Wheel-INS is less than 2% of the total traveled distance. We made the source code and data available to the community. (https://github.com/i2Nav-WHU/Wheel-INS)**

***Index Terms*—Dead reckoning; wheel-mounted IMU; MEMS IMU; wheeled robot; rotation modulation**

NOMENCLATURE

a) Matrices are denoted in uppercase bold letters.
b) Vectors are denoted in lowercase bold italic letters.
c) Scalars are denoted in lowercase italic letters.
d) Coordinate frames involved in the vector transformation are denoted as superscript and subscript. For vectors, the superscript denotes the projected coordinate system.
e) $\hat{*}$, estimated or computed values.
f) $\tilde{*}$, observed or measured values.
g) $\boldsymbol{a}_x$, element of vector $\boldsymbol{a}$ on the $\boldsymbol{x}$ axis.

I. INTRODUCTION

Positioning and heading estimation is an essential technology for autonomous mobile robots; it provides important information for the navigation and control system[1]. Current position tracking systems have relied heavily on the Global Navigation Satellite System (GNSS) and other radio signal-based techniques. Although GNSS can provide centimeter-level[2] positioning results in open-sky conditions, it deteriorates in complex environments such as urban canyons and forests owing to multipath and signal blockage. Moreover, it is completely unavailable for indoor navigation. Therefore, investigation of relative positioning methods to bridge GNSS outages is crucial to improve the robustness and reliability of the navigation system of mobile robots.

The last few years have witnessed the thriving development of visual sensor (e.g., camera and light detection and ranging (LiDAR))-based dead reckoning (DR) systems, such as simultaneous localization and mapping (SLAM)[3-5]. However, these systems are susceptible to external environments. For example, visual navigation systems suffer from illumination variation, motion blur, and high power consumption.

The inertial navigation system (INS) is a self-contained approach that shows significant superiority when considering system tolerance to disturbance in the surrounding environment. With the rapid development of microelectromechanical system (MEMS) technology, MEMS inertial measurement units (IMUs) have found wide application for motion detection, robot navigation, pedestrian dead reckoning (PDR) and more because of their small size, low cost, light weight, and low power consumption[6]. However, owing to the significant noise and bias instability of consumer-level MEMS IMUs, the positioning errors of INS-based DR systems drift quickly with time. Therefore, aiding information is required to suppress the error accumulation of INS.

The wheel odometer, a common sensor for ground wheeled robots, is extensively utilized to provide either distance or velocity information of the vehicle to suppress INS error drift because of its short-distance stability[7, 8]. It was proven that odometer and non-holonomic constraints (NHCs) contribute significantly to restrain both the positioning and attitude errors and enhance the INS stability[9, 10]. However, reliability of the odometer data depends on road conditions and vehicle maneuvers, which deteriorates if relative slippage occurs between the tires and contacting surface[8]. In addition, fusing information from different systems is challenging because of different standards, hardware modification, data transfer synchronization, and difficulties in obtaining reliability information along with the data[11].

There is wide agreement that multi-sensor integrated navigation is a key technology to meet the requirements of

This work was funded by the National Key Research and Development Program of China (No. 2016YFB0501800 and No. 2016YFB0502202). The authors are with the GNSS Research center, Wuhan University, Wuhan, China. {xjniu, ybwu, kuang}@whu.edu.cn.

precise, robust, and continuous positioning of mobile robots[1, 12, 13]. And inertial sensor lies at the heart of an integrated navigation system owing to its ability to continuously perceive three-dimensional (3D) motion and its independence from external environments and signals. As radio signals or environmental feature matching-based navigation techniques inevitably become unreliable and even fail in complex environments, the performance of INS-based DR systems (without external aiding information) must be improved to increase the reliability and usability of multi-sensor integrated navigation systems. It is worth mentioning that properly schemed motion of the IMU can effectively limit the error accumulation of INS, such as the carouseling IMU[14] or rotary INS[6, 15].

Rotation of the IMU with a constant angular rate can modulate the constant bias errors into periodic sinusoidal signals that can be canceled after integration over a complete rotation cycle[6]. However, an additional heavy, expensive, and sophisticated controllable rotation platform is required to perform the rotary INS; this negates the advantages. However, for a wheeled robot, the wheel is an inherent rotation device. Although the angular rate of the robot wheel cannot be controlled precisely, it can be approximated as constant during one cycle. Furthermore, by mounting a MEMS IMU on the wheel, the wheel velocity can be calculated using the gyroscope outputs and the wheel radius, which can replace the traditional wheel encoder or odometer. Moreover, a wheel-mounted MEMS IMU can be considered as a noninvasive sensor that adds almost no cost.

Few studies have been conducted with a focus on the wheel-mounted IMU-based navigation system. The most representative solution is a 2D DR system called PI-WMS developed by Collin[11, 16, 17]. In this system, the data of the two accelerometers, which are mounted perpendicular to the rotation axis, are used to determine the wheel rotation angle, which is multiplied by the wheel radius to obtain the travel distance; gyroscope outputs are utilized to calculate the vehicle heading. Although this system has evolved into a commercial product, the related algorithm has some deficiencies. First, the algorithm is based on the assumption of uniform vehicle motion, which is susceptible to continuous acceleration. In addition, the misalignment errors between the IMU and the wheel are not considered. If the measurement center of the IMU does not coincide with the wheel rotation center, the centripetal acceleration (which is related to the angular rate and position misalignment error) perceived by the accelerometer deteriorates the system performance.

In this study, a wheel-mounted MEMS IMU (Wheel-IMU)-based DR system (Wheel-INS) is proposed and implemented using an extended Kalman filter (EKF). Fig. 1 presents the algorithm flow. It should be noted that the DR system mentioned in this paper refers to the method of calculating the relative vehicle position with the pose increment, not just the traditional distance- and heading-based reckoning system. The forward INS mechanization is performed to predict the state of the Wheel-IMU. Moreover, the wheel velocity calculated by the gyroscope outputs and the wheel radius is treated as an external observation with NHCs to update the vehicle state. The state corrections estimated by the EKF are fed back to update the vehicle pose and compensate the IMU outputs.

The remainder of this paper is organized as follows. In Section II, the proposed installation scheme of the Wheel-IMU and its rotation characteristics are described first; then, the misalignment errors of the Wheel-IMU are defined and analyzed. Implementation details, including the error state model and observation model, of the proposed algorithm are presented in Section III. Experimental results are explained and discussed in Section IV. Section V provides some conclusions and directions for future work.

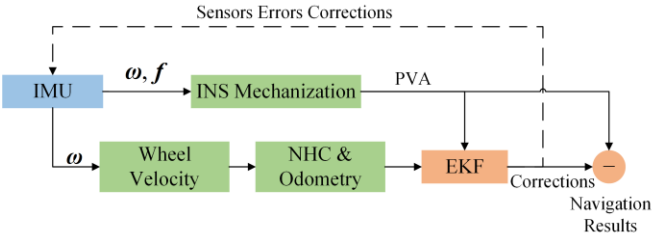

Fig. 1 Overview of the structure of the proposed Wheel-INS. $\boldsymbol{\omega}$ and $\boldsymbol{f}$ are the angular rate and specific force measured by the IMU, respectively; PVA means the position, velocity, and attitude of the IMU.

II. Prerequisites

Unlike the conventional odometer-aided INS (ODO/INS) in which the IMU is placed on the vehicle body or in the coach, in the proposed design, the IMU is mounted on a ground vehicle wheel to take advantage of the inherent rotation platform of the vehicle to mimic the rotary INS. In this section, the installation scheme of the Wheel-IMU and the coordinate systems involved in the Wheel-INS are introduced. Subsequently, the dynamic characteristics of the Wheel-IMU and the misalignment errors between the wheel and the Wheel-IMU are defined and analyzed.

A. Installation Scheme and Coordinate Systems

Fig. 2 illustrates the installation of the Wheel-IMU and the definition of the coordinate systems. To make the DR system indicate the vehicle state intuitively without being affected by vehicle maneuvers, the Wheel-IMU is placed on a non-steering wheel of the vehicle. The *v*-frame denotes the vehicle coordinate system, with the *x*-axis pointing to the advancement direction of the host vehicle, *z*-axis pointing down, and *y*-axis directing right to complete a right-handed orthogonal frame, i.e., forward-right-down. The origin of the *v*-frame is usually set at the vehicle mass center. The *w*-frame denotes the wheel coordinate system. Its origin is at the rotation center of the wheel. Its *x*-axis points to the right of the vehicle, and its *y*- and *z*-axes are parallel to the wheel surface to complete a right-handed orthogonal frame. The *b*-frame denotes the IMU coordinate system, in which the accelerations and angular rates generated by the strapdown accelerometers and gyroscopes are resolved[18]. The *b*-frame axes are the same as the IMU's body axes. The rotation axis is defined as the *x*-axis of the Wheel-IMU, pointing to the right of the

vehicle to avoid the singular pitch angle (±90°). Therefore, it can be considered that only the periodic rolling angle exists between the wheel coordinate system and the vehicle coordinate system for a vehicle with a stable structure. The heading difference between the Wheel-IMU and the vehicle can be approximated as fixed (equal to 90°).

$$\psi_b^n = \psi_v^n + \pi/2\,, \tag{1}$$

where ψ_b^n and ψ_v^n denote the IMU heading and vehicle heading, respectively. n indicates the n-frame, which is a local-level frame with origin coinciding with the b-frame, x-axis directs at the geodetic north, y-axis east, and z-axis downward vertically, i.e., the north-east-down system.

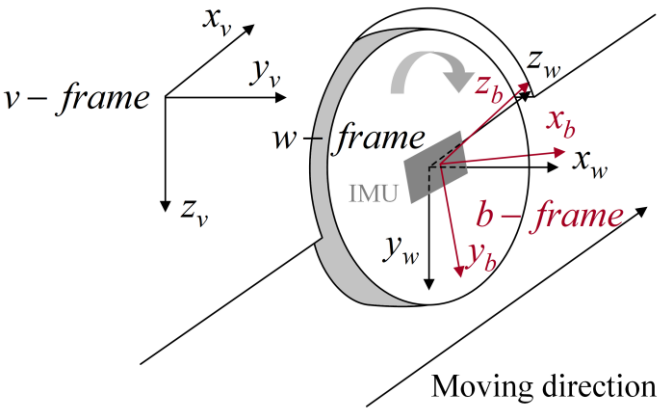

Fig. 2 Definition of the axis direction for the vehicle frame (v-frame), wheel frame (w-frame), and IMU body frame (b-frame). The position and attitude misalignment errors between the b-frame and the w-frame are also depicted.

B. Rotation of the Wheel-IMU

With the movement of the vehicle, the Wheel-IMU continuously rotates around the rotation axis of the wheel, i.e., the x_w axis in Fig. 2. Without loss of generality, we assume that the x-axis of the Wheel-IMU points to the north and the gyroscope bias and the rotation angular rate of the wheel remain constant in one rotation period of the wheel; this holds for normally moving robots and even low-end IMUs. As shown in equation (5), the INS attitude errors are correlated to the gyroscope measurement errors. Then, the IMU angular rate error projected to the n-frame can be written as

$$\begin{aligned}\mathbf{C}_b^n\delta\boldsymbol{\omega}_{ib}^b &= \begin{bmatrix}1 & 0 & 0\\ 0 & \cos\omega t & -\sin\omega t\\ 0 & \sin\omega t & \cos\omega t\end{bmatrix}\begin{bmatrix}\varepsilon_x\\ \varepsilon_y\\ \varepsilon_z\end{bmatrix}\\ &= \begin{bmatrix}\varepsilon_x\\ \varepsilon_y\cos\omega t-\varepsilon_z\sin\omega t\\ \varepsilon_y\sin\omega t+\varepsilon_z\cos\omega t\end{bmatrix}\end{aligned} \tag{2}$$

where ω is the IMU rotation rate, $\mathbf{C}_b^n$ is the rotation matrix from the b-frame to the n-frame, and $(\varepsilon_x \quad \varepsilon_y \quad \varepsilon_z)^{\mathrm{T}}$ are errors in the three gyroscope axes. The IMU attitude error caused by the gyroscope error can be obtained by integrating equation (2), i.e.,

$$\int_{Tc}\mathbf{C}_b^n\delta\boldsymbol{\omega}_{ib}^b = \begin{bmatrix}\int_{Tc}\varepsilon_x\\ \int_{Tc}\varepsilon_y\cos\omega t-\varepsilon_z\sin\omega t\\ \int_{Tc}\varepsilon_y\sin\omega t+\varepsilon_z\cos\omega t\end{bmatrix} = \begin{bmatrix}\int_{Tc}\varepsilon_x\\ 0\\ 0\end{bmatrix} \tag{3}$$

where Tc denotes the rotation period of the wheel. These equations show that because of the wheel rotation, the measurement error of the non-rotating axis of the gyroscope in the n-frame is modulated into a sine wave. After a period of integration, the accumulated pitch and heading error is zero. The IMU velocity errors caused by the accelerometer errors can be analyzed in the same way. A more detailed introduction of rotation modulation can be found in the literature[6, 19]. In conclusion, by rotating the IMU around a fixed axis, the IMU measurement errors caused by the attitude and velocity error in the other two axes of the Wheel-IMU are modulated into sinusoid signals. Thus, the velocity errors in the east and down directions, as well as the pitch and heading error caused by the error components that remain constant during one revolution of the wheel are canceled.

C. Misalignment Errors

As shown in Fig. 1, the gyroscope readings of the Wheel-IMU are utilized to calculate the wheel velocity to restrain the error accumulation of the INS with the NHCs in the Wheel-INS. Fusing the vehicle frame measurements with the INS requires knowledge of the installation relationship between the vehicle and the IMU. However, the misalignment problem is inevitable in any real system combining information from more than one sensor, which, if not handled properly, could noticeably decay system performance[20]. As depicted in Fig. 2, the misalignment errors include the position misalignment (called "lever arm"), pointing from the IMU center to the wheel rotation center expressed in the b-frame, and the attitude misalignment (called "mounting angles"), from the b-frame to the w-frame. The lever arm not only introduces errors to the projection of IMU velocity from the b-frame to the v-frame, but also introduces extra centripetal acceleration, which causes significant error in the DR system, especially when the vehicle moves at high speed. In practice, the lever arm can be determined by averaging multiple manual measurements. However, if the accuracy of the averaged results cannot meet the requirements, it can also be considered unknown parameters to be estimated online.

The attitude misalignment can be described as a set of Euler angles, $\Delta\phi$, $\Delta\theta$, and $\Delta\psi$, which can cause incomplete projection of the real wheel rotation angular rate on the x-axis of the gyroscope. In consequence, the calculated wheel velocity is smaller than the true value, which results in a scale error in the trajectory. However, because the ratio of the angular rate projection is the cosine of the mounting angle, the scale error is not evident when the mounting angles are small. Furthermore, equation (1) holds only when the mounting angles are effectively compensated. In addition, the attitude misalignment results in a periodic difference between the

calculated vehicle heading and the ground truth, because with the rotation of the wheel, the motion of the *x*-axis of the Wheel-IMU with respect to the *x*-axis of the *w*-frame forms a cone-shaped model. Because the roll mounting angle has no impact on the DR system, we consider only the pitch and heading misalignment angles. It worth mentioning that the attitude misalignment problem in the proposed Wheel-INS is similar to that of IMU-based pipeline inspection gauges (PIGs)[21, 22]. The authors in[22] proposed a complete method to calibrate the mounting angles between the PIG frame and the IMU body frame, in which details of the calibration procedure, error analysis, and more can be found. In our experiments, we used this approach to calibrate and compensate the mounting angles before data processing.

III. METHODOLOGY

Although the constant errors of the Wheel-IMU in the axis parallel to the wheel plane can be canceled by the rotation, errors in the rotation axis and other types of random error, particularly the accelerometer errors, can result in rapid position drift in the stand-alone INS. For this reason, other means are required to limit the error accumulation. Vehicle motion information (including wheel velocity and NHCs) are classic observations of vehicular navigation to fuse with INS. In this work, the Wheel-IMU gyroscope measurement and the wheel radius are used to calculate the wheel velocity without the need to install an external odometer or access the onboard odometer of the vehicle. Further, we selected the error-state EKF to implement the information fusion. In this section, the state model and the observation model of the proposed DR system are described.

A. Error State Model

In the Wheel-INS, conventional strapdown inertial navigation is utilized to predict the state of the IMU. The kinematic equations are described at length in the literature[7, 14, 23]; thus, we do not go into details here. The error-state Kalman filter is widely used in the navigation field to mitigate the nonlinearity problem. In this work, the state vector of the EKF constructed in the *n*-frame, including three dimensional position errors, three dimensional velocity errors, attitude errors, residual biases, and scale factor errors of the gyroscope and accelerometer, is written as

$$\boldsymbol{x}(t)=\left[\left(\delta\boldsymbol{r}_{INS}^{n}\right)^{\mathrm{T}}\quad\left(\delta\boldsymbol{v}_{INS}^{n}\right)^{\mathrm{T}}\quad\boldsymbol{\phi}^{\mathrm{T}}\quad\delta\boldsymbol{b}_{g}^{\mathrm{T}}\quad\delta\boldsymbol{b}_{a}^{\mathrm{T}}\quad\delta\boldsymbol{s}_{g}^{\mathrm{T}}\quad\delta\boldsymbol{s}_{a}^{\mathrm{T}}\right]^{\mathrm{T}} \tag{4}$$

where δ denotes the uncertainty of the variables; $\delta\boldsymbol{r}^{n}$, $\delta\boldsymbol{v}^{n}$, and $\boldsymbol{\phi}$ are the INS indicated position, velocity, and attitude errors, respectively; $\delta\boldsymbol{b}_{g}$ and $\delta\boldsymbol{b}_{g}$ are the residual bias errors of the gyroscope and the accelerometer, respectively; $\delta\boldsymbol{s}_{g}$ and $\delta\boldsymbol{s}_{a}$ are the residual scale factor errors of the gyroscope and accelerometer, respectively. Because of the errors from the sensors, IMU initial state, and other sources, the navigation parameters calculated by the INS mechanization equations contain errors. Several models have been developed to describe the time-dependent behavior of these errors[7]; the Phi-angle model was applied here, which can be written as

$$\dot{\boldsymbol{\phi}}=-\boldsymbol{\omega}_{in}^{n}\times\boldsymbol{\phi}-\mathbf{C}_{b}^{n}\delta\boldsymbol{\omega}_{ib}^{b} \tag{5}$$

$$\delta\dot{\boldsymbol{v}}^{n}=\mathbf{C}_{b}^{n}\delta\boldsymbol{f}^{b}+\mathbf{C}_{b}^{n}\boldsymbol{f}^{b}\times\boldsymbol{\phi}+\delta\boldsymbol{g}^{n} \tag{6}$$

$$\delta\dot{\boldsymbol{r}}^{n}=\delta\boldsymbol{v}^{n} \tag{7}$$

where $\boldsymbol{\omega}_{in}^{n}$ is the angular rate vector of the *n*-frame with respect to the inertial coordinates projected to the *n*-frame, which is calculated by $\boldsymbol{\omega}_{in}^{n}=\boldsymbol{\omega}_{ie}^{n}+\boldsymbol{\omega}_{en}^{n}$; e is the Earth-centered Earth-fixed coordinates; $\delta\boldsymbol{\omega}_{ib}^{b}$ and $\delta\boldsymbol{f}^{b}$ are the error vectors of the gyroscope and accelerometer, respectively, which can be expressed as $\delta\boldsymbol{\omega}_{ib}^{b}=\boldsymbol{b}_{g}+diag(\boldsymbol{\omega}_{ib}^{b})\boldsymbol{s}_{g}$ and $\delta\boldsymbol{f}^{b}=\boldsymbol{b}_{a}+diag(\boldsymbol{f}^{b})\boldsymbol{s}_{a}$; $diag(\bullet)$ is the diagonal matrix form of a vector; $\delta\boldsymbol{g}^{n}$ is the local gravity error in the *n*-frame. The sensor errors must be modeled to be augmented into the state vector. In this study, we chose the first-order Gauss-Markov process[24, 25] to model the sensor errors. The continuous-time model and discrete-time model are written as

$$\begin{aligned}\dot{x}&=-\frac{1}{T}x+w\\ x_{k+1}&=e^{-\Delta t_{k+1}/T}x_{k}+w_{k}\end{aligned} \tag{8}$$

where x is the random variable, T is the correlation time of the process, and w is the driving white noise.

Owing to the rotation of the wheel, the *y*-axis and *z*-axis change their directions around the *x*-axis periodically; thus, it is difficult for the Kalman filter to distinguish and estimate the sensor errors in these two axes effectively. However, the scale factor error of the gyroscope in the *x*-axis soon converges in the system, because it can be revealed clearly with the rotation of the wheel, whereas the gyroscope scale factor errors in the *y*-axis and *z*-axis are unobservable. Furthermore, the scale factor error of acceleration in the *y*-axis and *z*-axis can also be estimated jointly because they sense the gravity alternatively, and the horizontal motion assumption of the vehicle can make the errors evident.

Although estimating only the observable states in the Wheel-INS may reduce some computation cost, the cross-coupling errors of the MEMS inertial sensor triads couple the three axis errors together; thus, system performance degrades if we ignore the unobservable errors in a certain axis from the state vector, e.g., by estimating the scale factor error of the gyroscope only in the *x*-axis, not the *y*- and *z*- axes. A performance comparison of the Wheel-INS based on different dimensional state vectors and the square root of the variance of the IMU error estimation are shown in Section IV-B. The results show that the 21-state has better positioning performance. Therefore, the 21-state was structured in the Wheel-INS.

It is worth mentioning that the scale factor error of the wheel may degrade the performance of the Wheel-INS in some cases, and it cannot be substituted by other error states in the EKF because they impact the navigation results in different ways. The scale factor error of the wheel should be estimated online if other absolute positioning information is available, such as that of GNSS.

B. Observation Model

The wheel velocity indicated by the Wheel-IMU can be written as

$$\begin{aligned}\tilde{v}^v_{wheel} &= \tilde{\omega}_x r - e_v = (\omega_x + \delta\omega_x) r - e_v \\ &= v^v_{wheel} + r\delta\omega_x - e_v\end{aligned} \tag{9}$$

where $\tilde{\omega}_x$ is the gyroscope output in the x-axis, ω_x is the true value of the angular rate in the *x*-axis of the IMU, r is the wheel radius, and e_v is the observation noise, modeled as Gaussian white noise. As discussed in Section II-*C*, if the mounting angles are not compensated in advance, systematic deviation will occur between $\tilde{\omega}_x$ and ω_x, which causes scale errors in the result.

The motion of wheeled robots is generally governed by two NHCs[20, 26], which refers to the fact that the velocity of the robot in the plane perpendicular to the forward direction is almost zero when the robot does not slide on the ground or jump off the ground[7, 27]. By integrating with the NHCs, the 3D velocity observation can be expressed as

$$\tilde{\boldsymbol{v}}^v_{wheel} = \begin{bmatrix}\tilde{v}^v_{wheel} & 0 & 0\end{bmatrix}^{\mathrm{T}} - \boldsymbol{e}_v \tag{10}$$

Because the Wheel-IMU rotates with the wheel, the roll angle of the Wheel-IMU with respect to the wheel changes periodically. Consequently, the attitude of the vehicle cannot be obtained when projecting the observed velocity (which is in the *v*-frame) to the *n*-frame without other information. That is, it cannot be determined whether the vehicle is moving uphill or downhill by the Wheel-IMU alone. Therefore, we must assume that the vehicle is moving on a level surface. However, this assumption does not cause significant error to the DR system, as illustrated by the experiments described in Section IV. According to equation (1), the Euler angles of the vehicle can be represented as

$$\boldsymbol{\varphi}^n_v = \begin{bmatrix}\phi^n_v \\ \theta^n_v \\ \psi^n_v\end{bmatrix} = \begin{bmatrix}0 \\ 0 \\ \psi^n_b - \pi/2\end{bmatrix} \tag{11}$$

where ϕ, θ, and ψ are the roll, pitch, and heading angle, respectively. The corresponding rotation matrix can be calculated by

$$\mathbf{C}^v_n = \begin{bmatrix}\cos\psi^n_v & -\sin\psi^n_v & 0 \\ \sin\psi^n_v & \cos\psi^n_v & 0 \\ 0 & 0 & 1\end{bmatrix} \tag{12}$$

By performing perturbation analysis, the INS-indicated velocity in the *v*-frame can be written as

$$\begin{aligned}\hat{\boldsymbol{v}}^v_{wheel} &= \hat{\mathbf{C}}^v_n \hat{\boldsymbol{v}}^n_{IMU} + \hat{\mathbf{C}}^v_n \hat{\mathbf{C}}^n_b \left(\hat{\boldsymbol{\omega}}^b_{nb}\times\right)\boldsymbol{l}^b_{wheel} \\ &\approx \mathbf{C}^v_n \left(\mathbf{I} + \delta\boldsymbol{\psi}\times\right)\left(\boldsymbol{v}^n_{IMU} + \delta\boldsymbol{v}^n_{IMU}\right) \\ &\quad + \mathbf{C}^v_n \left(\mathbf{I} + \delta\boldsymbol{\psi}\times\right)\left(\mathbf{I} - \boldsymbol{\phi}\times\right)\mathbf{C}^n_b \left(\boldsymbol{\omega}^b_{nb}\times + \delta\boldsymbol{\omega}^b_{ib}\times\right)\boldsymbol{l}^b_{wheel} \\ &\approx \boldsymbol{v}^v_{wheel} + \mathbf{C}^v_n \delta\boldsymbol{v}^n_{IMU} + \mathbf{C}^v_n \left[\left(\mathbf{C}^n_b \left(\boldsymbol{\omega}^b_{nb}\times\right)\boldsymbol{l}^b_{wheel}\right)\times\right]\boldsymbol{\phi} \\ &\quad - \mathbf{C}^v_n \left[\left(\boldsymbol{v}^n_{IMU}\times\right) + \left(\mathbf{C}^n_b \left(\boldsymbol{\omega}^b_{nb}\times\right)\boldsymbol{l}^b_{wheel}\right)\times\right]\delta\boldsymbol{\psi} \\ &\quad - \mathbf{C}^v_n \mathbf{C}^n_b \left(\boldsymbol{l}^b_{wheel}\times\right)\delta\boldsymbol{\omega}^b_{ib}\end{aligned} \tag{13}$$

where $\mathbf{C}^v_n$ is the rotation matrix from the *n*-frame to the *v*-frame, which can be transformed from the Euler angles $\boldsymbol{\varphi}^n_v$ by equation (12); $\boldsymbol{\omega}^b_{nb}$ is the angular rate vector of the *b*-frame with respect to the *n*-frame projected to the *b*-frame; $\boldsymbol{l}^b_{wheel}$ indicates the lever arm vector between the Wheel-IMU and the *w*-frame projected in the *b*-frame; and $\delta\boldsymbol{\psi}$ is the attitude error of the vehicle, which is related only to the heading error in the state vector. Thus, it can be written as $\delta\boldsymbol{\psi} = [0 \quad 0 \quad \delta\psi^n_b]^{\mathrm{T}}$. Then, the velocity error measurement equation in the *v*-frame can be written as

$$\begin{aligned}\delta \mathrm{z}_v &= \hat{\boldsymbol{v}}^v_{wheel} - \tilde{\boldsymbol{v}}^v_{wheel} \\ &= \mathbf{C}^v_n \delta\boldsymbol{v}^n_{IMU} + \mathbf{C}^v_n \left[\left(\mathbf{C}^n_b \left(\boldsymbol{\omega}^b_{nb}\times\right)\boldsymbol{l}^b_{wheel}\right)\times\right]\boldsymbol{\phi} \\ &\quad - \mathbf{C}^v_n \left[\left(\boldsymbol{v}^n_{IMU}\times\right) + \left(\mathbf{C}^n_b \left(\boldsymbol{\omega}^b_{nb}\times\right)\boldsymbol{l}^b_{wheel}\right)\times\right]\delta\boldsymbol{\psi} \\ &\quad - \mathbf{C}^v_n \mathbf{C}^n_b \left(\boldsymbol{l}^b_{wheel}\times\right)\delta\boldsymbol{\omega}^b_{ib}\end{aligned} \tag{14}$$

Although the heading error can be limited effectively by the continuous rotation with the wheel, it accumulates rapidly when the vehicle remains stationary for a long time. In this case, zero-integrated heading rate measurements (ZIHRs)[7] can be performed to correct the heading. It is worth mentioning that the Wheel-IMU is more sensitive to vehicle motion; hence, it can perceive the vehicle motion more accurately than an IMU placed on the vehicle body.

IV. Experimental Results

This section provides and discusses the experimental results to illustrate the positioning performance of the Wheel-INS and the analysis of its characteristics. First, we discuss the key characteristics of the Wheel-INS by one test, including the mounting angles and the state dimension's influence on the navigation results, as well as the Wheel-INS's insensitivity to constant gyroscope bias. Then, we discuss the performance evaluation of the Wheel-INS compared with that of a conventional ODO/INS through multiple sets of experiments with different vehicles and environments.

A. Experimental Description

Field tests were conducted in three different scenarios in Wuhan City, China, using two different vehicles. One was the Pioneer 3DX robot, a typical differential wheeled vehicle, and the other was an ordinary car. The Pioneer robot was used for two tests and the car for one. Fig. 3 shows the experimental platforms.

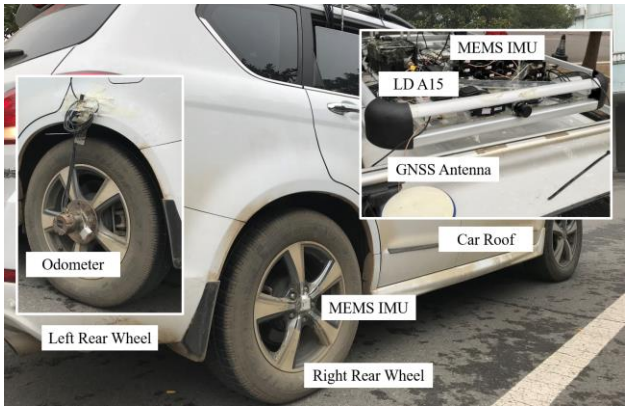

(a)

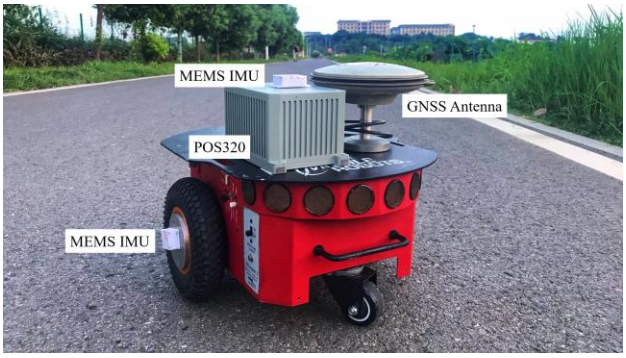

(b)

Fig. 3 Test platforms: (a) car; (b) Pioneer 3DX robot.

The MEMS IMU used in the experiments was self-developed and included four ICM20602 inertial sensor chips. We collected the outputs of two chips in one trajectory as two sets of experimental data for post-processing. The MEMS IMU was powered by a built-in battery and included a Bluetooth module inside it for time synchronization. The MEMS IMUs were carefully placed on the wheel to make them as close as possible to the wheel center. To compare its performance with that of a conventional ODO/INS, an identical MEMS IMU was placed on the vehicle body and wheel odometer data was recorded in every experiment. For the robot, the wheel speed data came from the motor; for the car, the wheel speed data came from an externally installed odometer. The root-mean-squared error (RMSE) of the wheel velocity measurements of the two vehicles were 0.03 m/s and 0.08 m/s, respectively. As shown in Fig. 3, the two vehicles were also equipped with two high-precision IMUs to provide pose ground truth: a POS320 (MAP Space Time Navigation Technology Co., Ltd., China) for the robot experiments and an LD A15 (Leador Spatial Information Technology Co., Ltd., China) for the car experiment. Their main technique parameters are listed in TABLE I. The reference data were processed through a smoothed post-processed kinematic (PPK)/INS integration method.

TABLE I
TECHNICAL PARAMETERS OF THE IMUS USED IN THE EXPERIMENTS

IMU	ICM20602	POS320	LD A15
Gyro Bias ($\deg/h$)	200	0.5	0.02
Angle Random Walk ($\deg/\sqrt{h}$)	0.24	0.05	0.003
Accelerometer Bias (m/s^2)	0.01	0.00025	0.00015
Velocity Random Walk ($m/s/\sqrt{h}$)	3	0.1	0.03

Fig. 4 shows the three test trajectories. Track I is a loopback trajectory in a small-scale environment, on which the robot moved approximately five times. Track II is a polyline trajectory with no return. Track III is a large loop trajectory on the whole campus, on which the robot moved approximately two times. The vehicle motion information of all the six tests is presented in TABLE II.

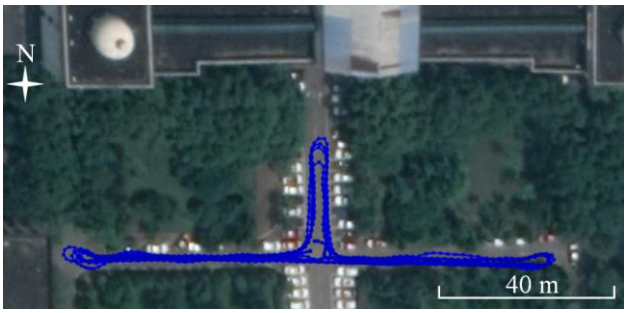

(a)

(b)

(c)

Fig. 4 Experimental trajectories in the (a) Information Department of Wuhan University, (b) Huazhong Agriculture University, and (c) Wuhan University campus.

TABLE II
VEHICLE MOTION INFORMATION IN THE EXPERIMENTS

Test	Track	Vehicle	Average Speed (m/s)	Total Distance (m)
1	I	Pioneer 3DX	1.39	≈1227
2				
3	II		1.25	≈1146
4				
5	III	Car	4.70	≈12199
6				

Because the attitude misalignment was compensated in advance, the initial heading and position of the Wheel-INS were given by the reference system directly. We chose this simple method for the initial alignment of the INS because we

focused mainly on the DR performance of the Wheel-INS. However, other alignment methods should be investigated for practical applications. The static IMU data before the vehicle started moving were used to obtain the initial roll and pitch, as well as the initial value of gyroscope bias.

B. Results and Discussion

1) Influence of Mounting Angles

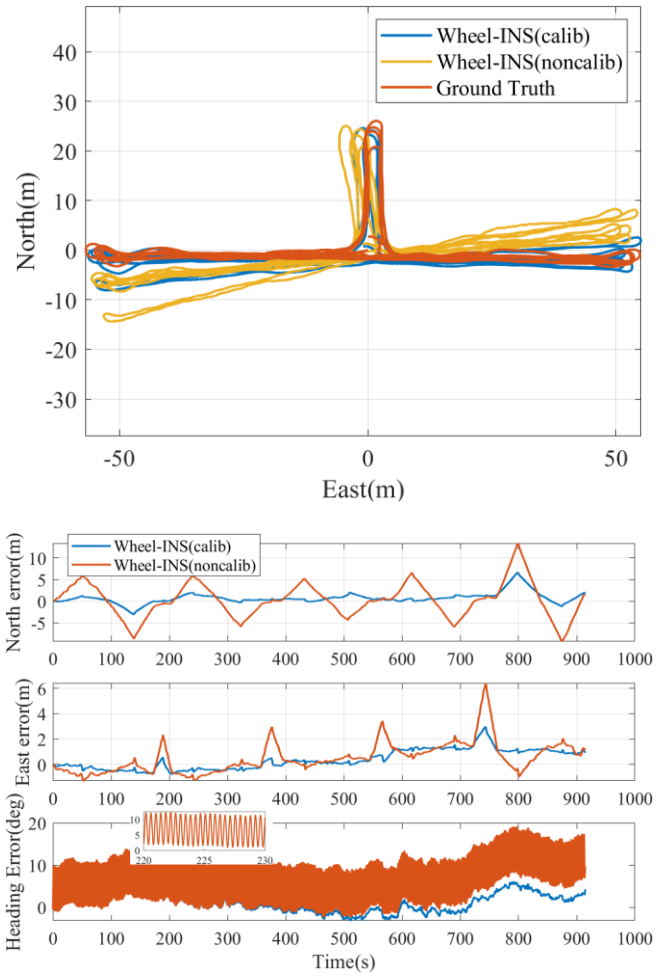

Fig. 5 Calculated trajectory, position errors in the north-east plane, and heading error of the Wheel-INS in Test 1. “calib” indicates that the IMU mounting angles were calibrated and compensated, whereas “noncalib” indicates that they were not compensated.

Fig. 5 shows the calculated vehicle trace, positioning errors in the north and east direction, and the heading error in Test 1 before and after compensating the mounting angles. The estimated values of the heading and pitch mounting angle were −4.5° and 2.5°, respectively. It can be observed that the positioning performance deteriorates significantly when the mounting angles of the Wheel-IMU are not compensated in advance. As discussed in Section II-*C*, the reason is that the mounting angles invalidate equations (1) and (11), thereby introducing errors to the positioning results when fusing INS with the wheel velocity and the NHCs. From equation (13) we learn that when the mounting angles are the same, a higher vehicle velocity corresponds with a larger error of the INS indicated wheel velocity in the *v*-frame. As shown in the second subplot of Fig. 5, when the mounting angles are not compensated in advance, a sine signal is modulated on the heading result, because the heading axis (*x*-axis) of the Wheel-IMU is not parallel to the rotation axis of the wheel, and the difference between them changes periodically with wheel rotation.

2) Insensitivity to Constant Gyroscope Bias

To prove the cancellation effect of rotation on constant gyroscope bias in the Wheel-INS, we conducted a contrast experiment in which the initial gyroscope bias was not set by the static data in Test 1, and then its performance was compared with that of a system in which the initial gyroscope bias was given. As shown in Fig. 6, there is no clear difference in the positioning errors between the two tests. However, the gyroscope bias caused a heading deviation when the vehicle started to move, as shown in the third subplot of Fig. 6, because the vehicle velocity was very low at that time; thus, the cancellation is not evident. However, when the speed increased, the heading drift caused by the constant bias was suppressed effectively. As the gyroscope bias cannot be effectively estimated by integrating vehicle frame measurements in a conventional ODO/INS, it can cause significant heading drift. However, the constant gyroscope bias does not degrade the performance of the Wheel-INS because of the rotation modulation. Therefore, the Wheel-INS is more insensitive to the constant gyroscope bias than is the ODO/INS.

Although zero-velocity updates (ZUPTs)[7, 28] and ZIHRs also benefit the estimation of the gyroscope bias, they are merely random signals that cannot be relied on. In addition, mistakes in detecting the static time interval of the vehicle undermine the stability of the system.

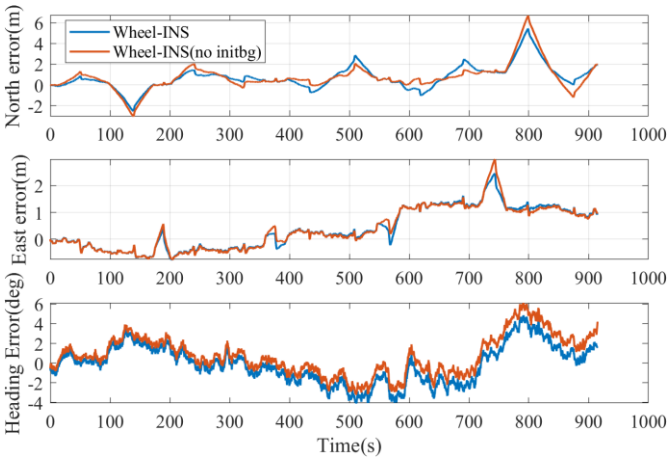

Fig. 6 Navigation error comparison of the Wheel-INS with and without giving the initial gyroscope bias in Test 1. “no initbg” indicates that the constant gyroscope bias was not calculated by the static data before data processing.

3) Why 21 Dimensions?

As discussed in Section III-*A*, we chose the 21-, 15-, and 9-dimensional state vectors in the Wheel-INS respectively in Test 1 to compare their positioning performance. The 15-state does not include the scale factor error of the gyroscope and accelerometer, and the 9-state does not include all the IMU

error terms. The corresponding navigation errors of the three experiments are shown in Fig. 7.

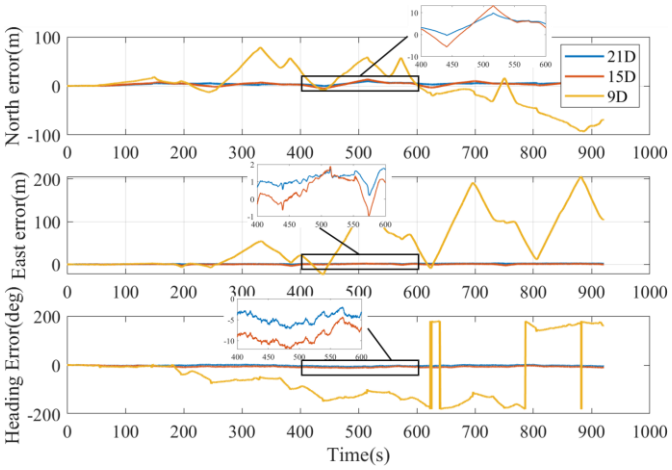

Fig. 7 Comparison of navigation errors of the Wheel-INS with different dimensions of state vector in Test 1. "21D," "15D," and "9D" indicate the 21-, 15-, and 9-state Wheel-INS, respectively.

It can be observed from Fig. 7 that the positioning error significantly increases when the dimension of the state vector is reduced to 9; the performance of the 15-state Wheel-INS is worse than that of the 21-state Wheel-INS. Although the constant bias of the IMU in the axis perpendicular to the rotation axis can be canceled to some extent, other error components can cause large error in the navigation results if they are not estimated and compensated. For example, the cross-coupling errors are more significant in the Wheel-INS because the dynamic condition of the Wheel-IMU is considerably higher than that of the traditionally placed IMU in vehicular navigation.

Fig. 8 depicts the square root of the variance of the inertial sensor errors estimation of the 21-state Wheel-INS in Test 1.

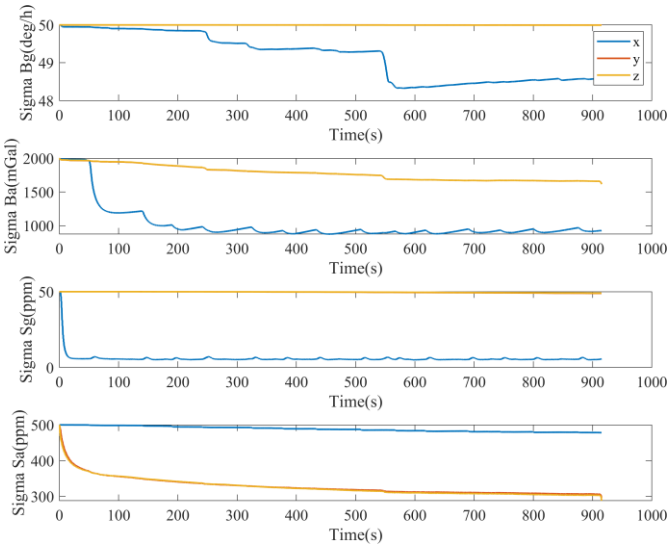

Fig. 8 Square root of variance of the inertial sensor residual error estimation of the Wheel-INS in Test 1.

As discussed in Section III-*A*, the IMU errors in the *y*- and *z*-axes are coupled together because they are parallel to the wheel plane, and change their directions periodically with the wheel, making it difficult for the filter to distinguish them. This effect explains why the curves of the errors in the *y*- and *z*-axes are almost coincident in all the subplots in Fig. 8. With regard to the scale factor error, because the Wheel-IMU rotates around the *x*-axis, a large rotation angular rate makes the gyroscopes scale factor error in the *x*-axis highly apparent. Therefore, it can soon converge in the system. In addition, as the wheel rotates, the accelerometers in the *y*- and *z*-axes perceive gravity alternatively. In addition, because of the vehicle horizontal motion assumption, the accelerometer scale factor errors in the *y*- and *z*-axes can be estimated by the Wheel-INS.

4) Performance Comparison

The vehicle trace, positioning error in the north and east direction, and heading error of the Wheel-INS in Test 3 and Test 7 are shown in Fig. 9 and Fig. 10, respectively. Calculating the closure error or the maximum position drift for the entire trajectory to demonstrate the positioning performance of a DR system is not optimal, because the loop of the trajectory will suppress error accumulation to some extent, especially for an INS in which the error drifts in one direction for a period of time. It can be observed from Fig. 5 and Fig. 10 that when the robot turns around, the positioning error starts to drift in the opposite direction. Therefore, we accumulated the moving distance of the robot by a certain increment (l) and calculated the maximum horizontal position error drift rate within each distance ($l, 2l, 3l, \ldots$). Next, the mean value (MEAN) and standard deviation (STD, 1σ) were computed as the final indicator of positioning performance. This approach is similar to the odometry evaluation metric proposed in the KITTI dataset[29], but we segmented the trajectory only from the starting point. With regard to the heading error, the maximum (MAX) and RMSE were calculated. In this work, we chose l as 100 m. TABLE III lists the error statistics of all the six experiments.

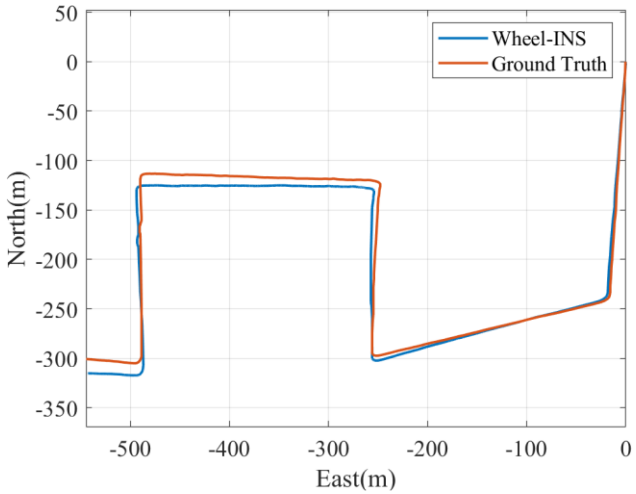

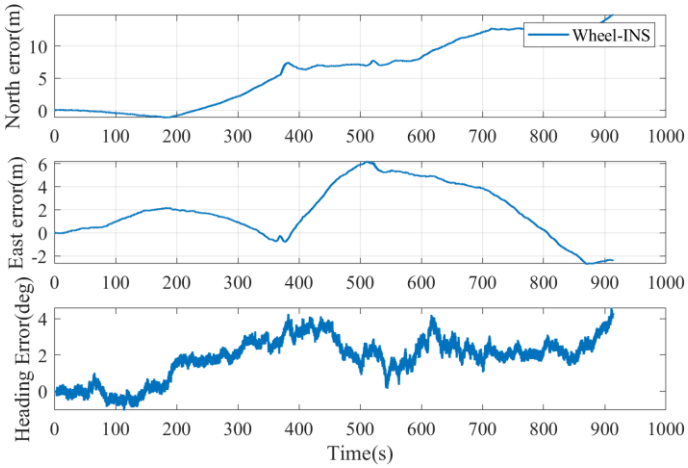

Fig. 9 Calculated trajectory, position errors in the north-east plane, and heading error of the Wheel-INS in Test 3.

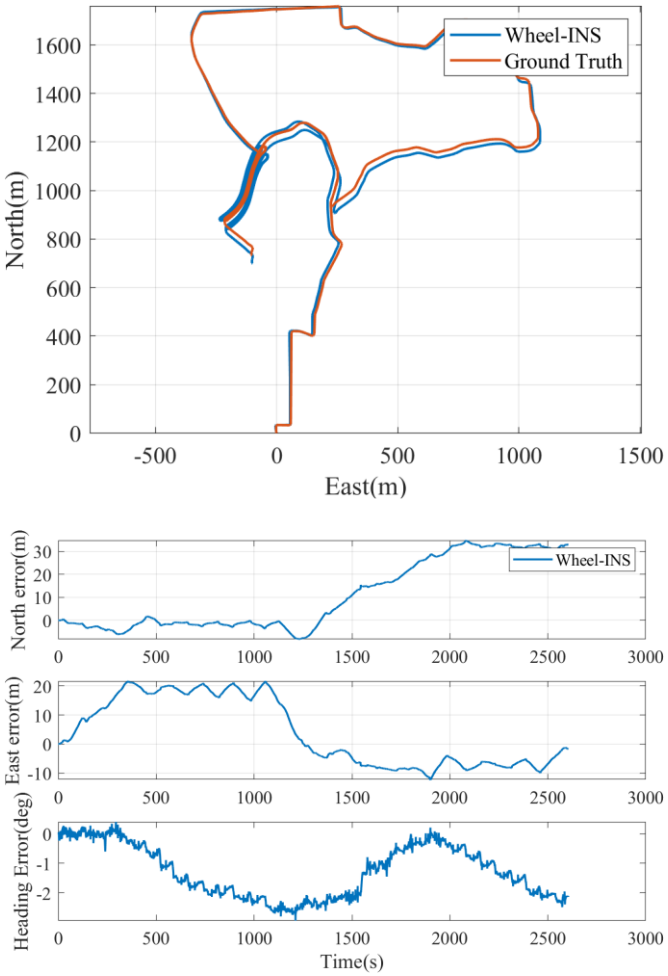

Fig. 10 Calculated trajectory, position errors in the north-east plane, and heading error of the Wheel-INS in Test 5.

TABLE III
PERFORMANCE COMPARISONS

Test No.	Algorithm	Position Drift Rate (%)		Heading Error (°)	
		MEAN	STD	MAX	RMS
1	Wheel-INS	0.59	0.30	4.79	1.93
	ODO/INS	0.58	0.45	5.11	2.11
2	Wheel-INS	1.43	0.54	7.93	3.88
	ODO/INS	0.57	0.32	4.79	2.82
3	Wheel-INS	1.17	0.27	4.56	2.16
	ODO/INS	2.25	0.68	8.00	2.88
4	Wheel-INS	1.78	0.26	10.88	4.44
	ODO/INS	2.20	0.88	9.87	5.77
5	Wheel-INS	0.62	0.42	1.91	0.96
	ODO/INS	1.14	0.65	3.30	1.38
6	Wheel-INS	0.83	0.43	4.97	1.60
	ODO/INS	1.62	1.04	6.72	2.65

From these results, the following information can be obtained.

- In all six experiments, the horizontal position drift rate of the Wheel-INS was between 0.60% and 1.90%, and the STD (1σ) was between 0.28% and 0.55%.
- In Test 1 and Test 2, the mean position drift error of the Wheel-INS was larger than that of the ODO/INS, whereas it was the opposite in other tests. After calculating the initial value of gyroscope bias by IMU data in the static period of the vehicle, the gyroscope bias remained stable for a short period of time (e.g., 15 min for Track I); therefore, the heading drift of the ODO/INS was small. However, there were many bumpy sections in Track II and Track III. In these situations, the IMU data vibrated violently and the NHC did not hold. In addition, because the lever arm between the wheel center and the IMU attached on the vehicle body was larger than that in the Wheel-INS, a greater error was generated during the velocity projection when fusing vehicle velocity with the INS, and in consequence the positioning error of ODO/INS was larger than that of the Wheel-INS.
- In Track III, the car moved in a large-scale environment with many continuous uphill and downhill roads (the maximum gradient was 10°), but the positioning accuracy of the Wheel-INS was admirable in Test 3 and Test 4. This result indicates that although the horizontal motion assumption of the vehicle is required, the Wheel-INS has a certain level of tolerance to sloping roads.
- The positioning errors of Test 3 and Test 4 are more significant than those of Test 1 and Test 2. The main reason for this result is that the positioning error cannot be canceled by loop closure in Test 3 and Test 4, because the shape of Track II is polyline. In contrast, in Test 1 and Test 2, the

positioning drift rate decreases with increasing distance owing to the loop closure.

- The performance of the Wheel-INS in the car experiments was better than that of robot experiments for both positioning and heading. It is evident that the wheel structure of a car is substantially more stable than that of a mobile robot. Moreover, it can be observed from TABLE II that the car moved faster than the robot in the tests. In other words, the Wheel-IMU attached on the car spins more times in the same amount of time. Therefore, the effect of rotation modulation is more evident to some extent, resulting in higher accuracy in heading.
- Under ideal conditions, e.g., given the initial gyroscope bias, and with the vehicle moving on flat road, the performance of the Wheel-INS is at the same level as that of the ODO/INS.

V. Conclusion

A novel and complete DR solution based on the Wheel-IMU is proposed in this study. The key objective in this system is to take advantage of the inherent rotation platform of the wheeled robot to spread the INS drift errors to all directions and realize the cancellation effect, to improve the heading accuracy as well as mitigate the positioning drift.

The misalignment errors of the Wheel-IMU are defined and analyzed; they must be compensated in advance to obtain more robust and precise navigation results. Owing to the rotation modulation effect, the Wheel-INS is insensitive to the constant gyroscope bias.

Furthermore, the observability of the sensor errors in the state vector are analyzed by their covariance propagated in the EKF algorithm. Because the residual error of the inertial sensors in the directions perpendicular to the rotation axis are coupled to each other owing to the continuous rotation, it cannot be distinguished and estimated by the EKF. However, the scale factor error of the gyroscope of the rotation axis can converge quickly in the system.

Experimental results show that the 21-state vector-based EKF can achieve better performance, because the couplings between the errors of different directions makes it necessary to estimate the errors in all three axes.

Field tests in different environments with different vehicles demonstrate that the MEMS IMU-based Wheel-INS has a maximum horizontal position drift of less than 2% of the total travel distance and exhibits the same performance as the conventional ODO/INS.

To promote the Wheel-INS solution in autonomous navigation application for wheeled robots, two problems must be solved: power supply and data transformation. Energy-harvesting techniques and Bluetooth communication can be considered to achieve an “install and forget” solution.

Future research directions include investigating approaches to use the vehicle attitude indicated by another IMU mounted on the vehicle body to extend the Wheel-INS from 2D positioning to 3D navigation. Furthermore, the use of two Wheel-IMUs mounted on left and right wheels is a promising approach for obtaining double information and take advantage of the spatial constraint between them to make the solution more robust.

Reference

[1] S. Kuutti, S. Fallah, K. Katsaros, M. Dianati, F. Mccullough, and A. Mouzakitis, "A survey of the state-of-the-art localization techniques and their potentials for autonomous vehicle applications," *IEEE Internet of Things Journal*, vol. 5, pp. 829-846, 2018.

[2] P. Teunissen and O. Montenbruck, *Springer Handbook of Global Navigation Satellite Systems*: Springer, 2017.

[3] H. Durrant-Whyte and T. Bailey, "Simultaneous localization and mapping: part I," *IEEE robotics & automation magazine*, vol. 13, pp. 99-110, 2006.

[4] T. Bailey and H. Durrant-Whyte, "Simultaneous localization and mapping: Part II," *IEEE robotics & automation magazine*, vol. 13, pp. 108-117, 2006.

[5] J. Zhang and S. Singh, "LOAM: Lidar Odometry and Mapping in Real-time," in *Robotics: Science and Systems*, 2014.

[6] S. Du, "Rotary inertial navigation system with a low-cost MEMS IMU and its integration with GNSS," Ph.D., University of Calgary, 2015.

[7] E. H. Shin, "Estimation techniques for low-cost inertial navigation," PhD, Department of Geomatics Engineering, The University of Calgary Calgary, Canada, 2005.

[8] Y. Wu, C. Goodall, and N. El-Sheimy, "Self-calibration for IMU/odometer land navigation: Simulation and test results," in *Proceedings of the ION International Technical Meeting, San Diego, CA, USA*, 2010.

[9] S. Godha, "Performance evaluation of low cost MEMS-based IMU integrated with GPS for land vehicle navigation application," *UCGE report*, 2006.

[10] G. Dissanayake, S. Sukkarieh, E. Nebot, and H. Durrant-Whyte, "The aiding of a low-cost strapdown inertial measurement unit using vehicle model constraints for land vehicle applications," *IEEE transactions on robotics and automation*, vol. 17, pp. 731-747, 2001.

[11] J. Collin, "MEMS IMU Carouseling for Ground Vehicles," *IEEE Transactions on Vehicular Technology*, vol. 64, pp. 2242-2251, 2015.

[12] DARPA. (2012, April 20). *All Source Positioning and Navigation (ASPN) Phase 2*. Available: https://govtribe.com/opportunity/federal-contract-opportunity/all-source-positioning-and-navigation-aspn-phase-2-darpabaa1245

[13] D. A. Grejner-Brzezinska, C. K. Toth, T. Moore, J. F. Raquet, M. M. Miller, and A. Kealy, "Multisensor Navigation Systems: A Remedy for GNSS Vulnerabilities?," *Proceedings of the IEEE*, vol. 104, pp. 1339-1353, 2016.

[14] P. D. Groves, *Principles of GNSS, inertial, and multisensor integrated navigation systems*: Artech house, 2013.
[15] E. S. Geller, "Inertial System Platform Rotation," *IEEE Transactions on Aerospace and Electronic Systems*, vol. AES-4, pp. 557-568, 1968.
[16] PISystems. (2019, April 19). Available: http://pacificinertial.com/products
[17] J. Collin, M. Kirkko-Jaakkola, and J. Takala, "Effect of Carouseling on Angular Rate Sensor Error Processes," *IEEE Transactions on Instrumentation and Measurement*, vol. 64, pp. 230-240, 2015.
[18] B. M. Scherzinger and D. B. Reid, "Modified strapdown inertial navigator error models," in *Proceedings of 1994 IEEE Position, Location and Navigation Symposium - PLANS'94*, 1994, pp. 426-430.
[19] K. A. Rahim, "Heading drift mitigation for low-cost inertial pedestrian navigation," University of Nottingham, 2012.
[20] Y. Wu, M. Wu, X. Hu, and D. Hu, "Self-calibration for land navigation using inertial sensors and odometer: Observability analysis," in *AIAA Guidance, Navigation, and Control Conference*, 2009, p. 5970.
[21] Q. Chen, Q. Zhang, X. Niu, and Y. Wang, "Positioning Accuracy of a Pipeline Surveying System Based on MEMS IMU and Odometer: Case Study," *IEEE Access*, vol. 7, pp. 104453-104461, 2019.
[22] Q. Chen, X. Niu, J. Kuang, and J. Liu, "IMU Mounting Angle Calibration for Pipeline Surveying Apparatus," *IEEE Transactions on Instrumentation and Measurement*, pp. 1-1, 2019.
[23] K. R. Britting, "Inertial navigation systems analysis," 1971.
[24] P. S. Maybeck, *Stochastic models, estimation, and control* vol. 1: Academic press, 1979.
[25] R. G. Brown and P. Y. Hwang, *Introduction to random signals and applied Kalman filtering* vol. 3: Wiley New York, 1992.
[26] R. Siegwart, I. R. Nourbakhsh, and D. Scaramuzza, *Introduction to autonomous mobile robots*: MIT press, 2011.
[27] S. Sukkarieh, "Low cost, high integrity, aided inertial navigation systems for autonomous land vehicles," University of Sydney Sydney, NSW, Australia, 2000.
[28] C. Kilic, J. N. Gross, N. Ohi, R. Watson, J. Strader, T. Swiger, *et al.*, "Improved Planetary Rover Inertial Navigation and Wheel Odometry Performance through Periodic Use of Zero-Type Constraints," presented at the IEEE/RSJ International Conference on Intelligent Robots and Systems (IROS) 2019, Macau, China, 2019.
[29] A. Geiger, P. Lenz, and R. Urtasun, "Are we ready for autonomous driving? The KITTI vision benchmark suite," in *2012 IEEE Conference on Computer Vision and Pattern Recognition*, 2012, pp. 3354-3361.